Fluorescence Spectroscopy of Conformational Changes of Single LH2 Complexes

Danielis Rutkauskas,* Vladimir Novoderezhkin,[†] Richard J. Cogdell,[‡] and Rienk van Grondelle*

*Department of Biophysics and Physics of Complex Systems, Division of Physics and Astronomy, Faculty of Sciences, Vrije Universiteit, 1081 HV Amsterdam, The Netherlands; [†]A. N. Belozersky Institute of Physico-Chemical Biology, Moscow State University, Moscow 119899, Russia; and [‡]Division of Biochemistry and Molecular Biology, Institute of Biomedical and Life Sciences, University of Glasgow, Glasgow G12 8QQ, United Kingdom

ABSTRACT   We have investigated the energy landscape of the bacterial photosynthetic peripheral light-harvesting complex LH2 of purple bacterium *Rhodopseudomonas acidophila* by monitoring sequences of fluorescence spectra of single LH2 assemblies, at room temperature, with different excitation intensities as well as at elevated temperatures, utilizing a confocal microscope. The fluorescence peak wavelength of individual LH2 complexes was found to abruptly move between long-lived quasi-stable levels differing by up to 30 nm. The frequency and size of these fluorescence peak movements were found to increase linearly with the excitation intensity. These spectral shifts either to the blue or to the red were accompanied by a broadening and decrease of the intensity of the fluorescence spectrum. The probability for a particle to undergo significant spectral shift in either direction was found to be roughly the same. Using the modified Redfield theory, the observed changes in spectral shape and intensity were accounted for by changes in the realization of the static disorder. Long lifetimes of the quasi-stable states suggest large energetic barriers between the states characterized by different emission spectra.

INTRODUCTION

Photosynthetic pigment-protein complexes play a decisive role in the collection of solar energy and the transfer of electronic excitation energy to the photosynthetic reaction center, where a charge separation is initiated (van Grondelle, 1985; van Grondelle et al., 1994). Since a high-resolution crystallographic structure of the peripheral light-harvesting complex LH2 of the photosynthetic bacterium *Rhodopseudomonas acidophila* has become available (McDermott et al., 1995; Papiz et al., 2003), the molecule has played a key role in aiding our current understanding of photosynthetic light-harvesting (Cogdell et al., 1996; Hu et al., 2002; Robert et al., 2003; Sundström et al., 1999). The LH2 of *Rps. acidophila* is a highly symmetric ring of nine protein-pigment subunits, each containing two helical transmembrane polypeptides: the α-polypeptide on the inner and the β-polypeptide on the outer side of the ring. The hydrophobic terminal of the protein binds a ring of 18 tightly coupled bacteriochlorophyll (BChl) molecules with a center-to-center distance of <1 nm between neighboring pigments. This ring is responsible for the intense absorption of LH2 at 850 nm (B850 ring). A second ring of nine weakly interacting BChls is located in the polar region of the protein and is largely responsible for the absorption around 800 nm (B800 ring).

From the detailed study of the spectroscopic properties of LH2, a consistent picture of energy levels and energy transfer in the complex has emerged (Alden et al., 1997; Hu et al., 1997; Novoderezhkin et al., 1999b, 2003; Sauer et al., 1996; Scholes and Fleming, 2000; van Grondelle and Novoderezhkin, 2001; Wu et al., 1997). All basic spectro-scopic features can be understood on the basis of a model that includes both intrinsic pigment site energy disorder and excitonic coupling between the pigments ($\sim$300 cm^{-1} for neighboring BChls in the B850 and $\sim$30 cm^{-1} for adjacent pigments in the B800). By introducing relaxation between the elements of the so-called density matrix, the dynamics of vibrational and electronic coherence and excitation energy transfer have been described in great detail.

Based on room and low temperature single-molecule experiments, it has been proposed that the LH2 ring can deviate from the ideally circular structure of the complex in crystal (Bopp et al., 1999; Ketelaars et al., 2001; Matsushita et al., 2001; van Oijen et al., 1999). The anomalously large splitting of the two major orthogonal excitonic transitions observed in low temperature polarized fluorescence (FL) excitation spectra was attributed to a modulation of the coupling strength in the B850 ring that was asserted to be associated with an elliptical deformation (Ketelaars et al., 2001; Matsushita et al., 2001; van Oijen et al., 1999). It was found that native membrane environment contributes signif-icantly to stabilization of the circular structure of bacterial light-harvesting complexes (Gerken et al., 2003). Thus smaller ellipticities of 0.95–0.91 were found in atomic force microscopy measurements of loosely packed LH2s in mem-brane, and were probably due to an interplay of the disrupt-ing tip and stabilizing lipid environment effects (Scheuring et al., 2001).

Room temperature (RT) polarized FL experiments were interpreted in terms of an elliptical absorber and emitter, with ellipticity and directions of the principal axis varying as a result of the B800 and/or B850 distortion destroying the rotational symmetry and traveling around the ring on

a timescale of seconds (Bopp et al., 1999). Spectral diffusion of the B800 band of LH2, observed in the low temperature experiments, was also attributed to structural alterations (van Oijen et al., 2000). These spectral fluctuations of different magnitude occurring on different timescales were associated with a hierarchical structure of the protein conformational landscape (Hofmann et al., 2003). In general, the observed variation of the spectral and functional properties of LH2 suggests that the complex can undergo a variety of deformations. It is in accordance with the widely excepted notion of a protein as a complex system that is characterized by a rugged potential energy landscape with multiple barriers separating potential energy valleys associated with different conformational substates (Frauenfelder, 2003). At RT, protein possesses sufficient energy to migrate between different substates. Protein transitions from one substate to another can be also induced by repetitive laser excitation due to thermal energy released through radiationless deactivation channels after pigment absorption of excitation light. In a pigment-protein complex like LH2, spectral peak positions and lineshapes of absorption and FL spectra are partly determined by the pigment-protein interactions such as through the formation of hydrogen bonds (Fowler et al., 1992; Olsen et al., 1994). The latter are modulated by the structural changes of the protein and so are the spectra. For a phenomenological description of the underlying electronic mechanism of spectral changes, it is reasonable to assume that dynamic structural alterations of the protein also underlie the pattern of the static disorder of the pigment site energies that play a key role in understanding of the spectroscopic and energy-transfer properties of LH2.

In this work we investigate these dynamic fluctuations under physiological conditions, as manifested by the time evolution of the FL spectrum. To do so, we have acquired a series of FL spectra of single LH2 complexes at room and elevated temperatures with various excitation intensities. We observed sudden moves of the peak position of the emission spectrum of LH2; both the frequency and the magnitude of spectral jumps were found to depend on the excitation intensity. Spectral jumps to the blue and to the red occur with a similar probability and are associated with spectral broadening and lowering of the intensity. The observed spectral variations can be qualitatively interpreted by sudden changes in the realization of the static disorder.

MATERIALS AND METHODS

Sample preparation and immobilization

Isolated LH2 complexes were immobilized on a standard microscope coverslip (0.17 mm thickness) treated with 0.01% poly-L-lysine (Sigma, St. Louis, MO) solution for 5 min. The coverslip was used as a base for a home-designed, hermetic, temperature-controlled sample cell.

Purified LH2 complexes of *Rps. acidophila* were prepared as described earlier (Cogdell and Hawthornthwaite, 1993; Halloren et al., 1995). The sample stock solution of 0.62 μM LH2 in buffer (20 mM Tris-HCl (pH 8.0)

and 0.1% lauryldimethylamine oxide (LDAO)) was kept at $-80°C$ before thawing. It was diluted in the same buffer in two steps by a factor of 2×10^4. A 20 μl drop of 33 pM LH2 solution was added onto the coverslip, and the sample cell was assembled. After a few minutes, the cell volume was washed with deoxygenated, 0.1% lauryldimethylamine oxide-containing buffer, thus removing the excess sample and submerging the immobilized single molecules in an oxygen-free environment. Oxygen was thoroughly removed from the buffer by flowing gaseous nitrogen and agitating with a magnetic spinner to the level not detectable by electrolytic oxygen meter (Cyberscan 100 Do, Eutech Instruments, Nijkerk, The Netherlands). Buffer was inserted into the sample cell directly from the deoxygenation volume with excessive gaseous nitrogen pressure. In this procedure, the use of chemical oxygen scavenger was avoided.

Experimental setup

FL images and spectra were acquired with a confocal microscope based on a commercial inverted microscope (Eclipse TE300, Nikon, Tokyo, Japan). A scheme of the setup is presented in Fig. 1. The excitation source was a tunable-wavelength Ti:sapphire laser system (Mira 900, Coherent, Santa Clara, CA) producing 3 ps, 800 nm pulses with a repetition rate of 76 MHz. A dichroic beam splitter (815dclp, Chroma Technology, Rockingham, VT) reflected the laser beam into an objective (Plan Fluor 100×, 1.3 NA, oil immersion, Nikon), focusing the excitation light onto a glass-water interface in the sample cell to a diffraction-limited spot (full width at half-maximum of ~600 nm). The intensities used in the experiments (from 0.13 to 1.6 kW/cm^2 or equivalently 500 nW–6 μW) represent the values at this interface. Nonfluorescing immersion oil (Nikon) coupled the objective to the glass coverslip. The emission was collected with the same objective and spatially filtered by a 100 μm pinhole. Scattered excitation light was rejected with single 130 nm broad interference filter (HQ885/130m, Chroma).

The sample cell was mounted on a closed-loop two-dimensional piezo stage (P-731.8C, Physik Instrumente, Waldbronn, Germany) controlled by a digital four-channel controller (E-710.4LC, Physik Instrumente).

To obtain images, emission was detected with Si avalanche photodiode single photon-counting module (SPCM-AQR-16, PerkinElmer Optoelectronics, Fremont, CA) and counter timer board (PCI-6602, National Instruments, Austin, TX). Spectra were acquired by dispersing the FL onto a liquid nitrogen-cooled back-illuminated charge-coupled device (CCD) camera chip (Spec10:100BR, Princeton Instruments, Roper Scientific, Princeton, NJ) by a gold-coated grating (HR600/1.0U 30SQ.X9.5mm, Optometrics, Ayer, MA). CCD pixels were binned along the spectroscopic axis to yield a resolution of <1nm. The polarization sensitivity of the detection was found to be insignificant and thus no correction was required. The setup was switched between the image acquisition and spectroscopic modes by a motorized mirror flipper (8892M, New Focus, San Jose, CA).

The longitudinal drift of the focus due to thermal flux in experiments at elevated temperature was eliminated by monitoring focus position with a monochrome video camera (Watec LCC-902K, Watec America, Las Vegas, NV) coupled to a video grabber board (PCI-1407, National Instruments) and translating the microscope objective with a motorized polarizer rotator (8401M, 8754 driver, New Focus) to optimum position after an acquisition of each series of FL spectra.

An electrical shutter (Uniblitz VS25S2S1, VMM-D1 driver, Vincent Associates, Rochester, NY) blocked the excitation light between the measurements.

Mirror and lens antireflection coatings were optimized for signal processing in near infrared.

Images and spectra

A FL image is acquired by continuously sweeping the piezo stage over the laser focus with the 3 Hz frequency while its position in the perpendicular direction is changed by 100 nm for each line; the FL signal is concomitantly
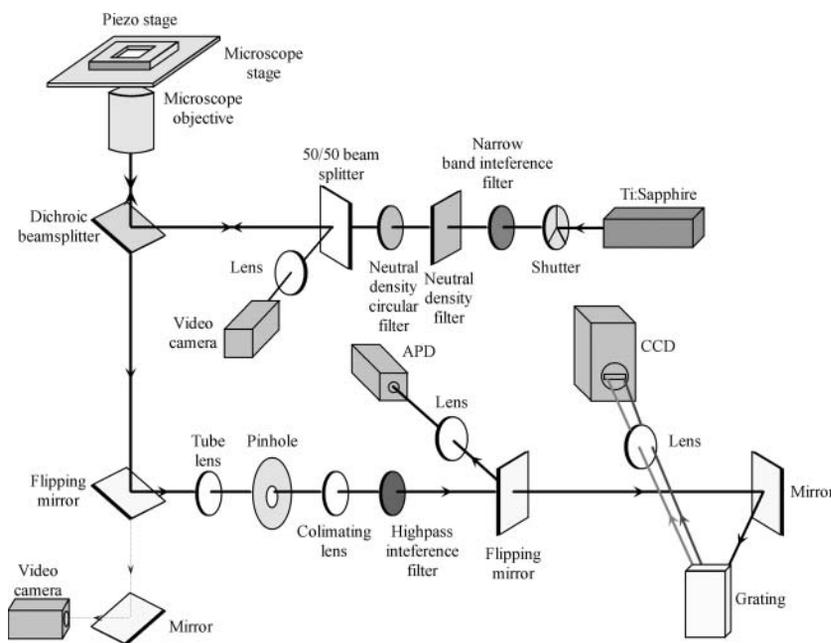
FIGURE 1 Optical scheme of the experimental setup.

detected with an avalanche photodiode. The image is then constructed by associating the piezo stage coordinate with the corresponding intensity. The scanning covers an area of 10 μm $\times$ 10 μm. The image is background-thresholded, and excessively small, big, bright, weak, elongated, or adjacent particles, as well as particles bordering the edges of the image, are discarded. The coordinates of remaining particles are determined, and the piezo stage is positioned to bring the particle into the focus of the objective, and after switching to the spectroscopic mode, a series of FL spectra is collected for 2 min with an integration time (0.5–2 s) dependent on the excitation power and the sample temperature. At higher excitation intensities and lower temperature, shorter integration times are sufficient for the collection of the spectra with satisfactory signal/noise ratio. The excitation intensity and the ambient conditions remain unchanged during the acquisition.

Bulk spectra were measured with the same setup on assemblies immobilized on a treated coverslip from the stock solution of LH2.

The spectrofluorometer was wavelength-calibrated by referencing the known lines of Ar lamp spectrum, acquired by positioning the lamp over a milk emulsion layer on a coverslip (creating a uniform light source) and focusing the microscope objective on the coverslip-water interface.

Detection sensitivity was calibrated with a tungsten halogen lamp, assuming that its emission spectrum is flat in the region of interest.

Software

The program communicating with the counter timer and video grabber boards, driving piezo stage, motorized flipper, electrical shutter, and motorized polarizer rotator was coded in the LabVIEW (National Instruments) environment. Commercial CCD camera software was accessed from the program, utilizing ActiveX technology (Microsoft, Redmond, WA).

Data analysis

For a quantitative analysis, the acquired spectra are fitted with a skewed Gaussian function, using a nonlinear Levenberg-Marquardt fitting method. The expression for the skewed Gaussian function is

$$F(\lambda) = \Delta + A \exp(-\ln(2)/b^2 \ln(1 + 2b(\lambda - \lambda_m)/\Delta\lambda))^2,$$

where Δ is the offset, A the amplitude, λ_m the FL peak (FLP) wavelength, $\Delta\lambda$ the width, and b the skewness. The full width at half-maximum (fwhm) of the spectrum is calculated from the width and the skewness. Consequently, by fitting each spectrum from a series, we obtain the time traces of the amplitude, the fwhm, and the FLP with the corresponding confidence margins.

RESULTS

The primary objective of this study was to investigate if we could observe fluctuations of peak position, width, and intensity of the emission spectrum of single LH2 complexes as a measure of structural dynamics, which can occur in this complex. This was achieved by collecting a series of single-molecule FL spectra at RT and variable excitation intensity as well as at elevated temperature. In total, close to 1000 molecules were studied at various ambient conditions. Intrinsic (i.e., measured with low excitation power) fluctuations proved to be insignificant on the timescale of our experiment (2 min). However, increasing the excitation power introduced prominent spectral jumps and changes in the spectral shape and intensity of the emission. To a smaller extent, the same effect was detectable in experiments at elevated temperatures (28, 35°C). However, under these conditions, the stability of the LH2 complexes was decreased significantly.

Earlier experiments (Bopp et al., 1999) have shown that the survival time of the illuminated LH2 complexes strongly depends on the presence of oxygen in the environment. We observed that irreversible photobleaching of an oxygen-containing sample took place in the course of seconds or tens of seconds, and even when kept in the dark, the oxygen-containing preparation degraded in a few hours at RT. On the

other hand, careful removal of oxygen from the sample ambient prolonged the bright state of single LH2s to minutes or even tens of minutes, and the sample remained suitable for measurements for 2 days.

Furthermore, at relatively low excitation intensity (500 nW), only ~20% of the molecules entered a dark state in the course of 2 min. The remaining 80% stayed bright during the measurement, and their emission intensity fluctuated between levels of different magnitude. This is in contrast to the earlier study (Bopp et al., 1997), where a larger fraction of particles bleached permanently or temporarily entered the dark state in a few seconds after the onset of the excitation—probably due to the remaining dissolved oxygen.

For the above reasons, all of the single-molecule measurements presented in this work were carried out on the oxygen-free samples.

Images

An example of a raw FL image of immobilized LH2 assemblies is shown in Fig. 2. The image consists of 100 pixels × 100 pixels; the pixel integration time is 3 ms. The excitation intensity at 800 nm is 3.5 μW. The background is ≤10 counts per pixel and the maximum intensity is 87 counts per pixel. Although particles appear to be of a similar integral intensity, in reality they are distributed over a range of 1300–2500 counts, which is probably partly due to the polarization effects of the excitation absorption and emission and partly to the tendency of the emission intensity to fluctuate. The latter consideration is supported by the fact that at lower excitation intensity levels, the distribution of the particle intensities is notably narrower. We also do not exclude the possibility of observing aggregated complexes or adjacent complexes appearing as one particle. To make sure that we monitor only single LH2s, excessively bright particles are discarded and spectral measurements are carried out on molecules that lie in the middle of the bulk of the intensity distribution.
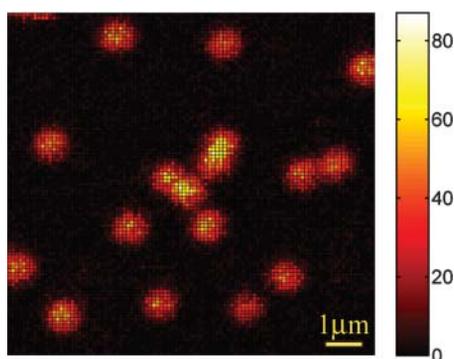
FL spectra

A typical series of FL spectra of single LH2, enabling the observation of the spectral diffusion, is presented in Fig. 3. These results where obtained from a sequence of 240 single LH2 spectra, acquired at 20°C with 0.5 s integration time and excitation intensity of 6 μW at 800 nm, by summing each 10 consecutive spectra for clarity. In this experiment, the FL amplitude and the FLP diffuse dramatically, with the integral intensity ranging from 4000 to 10000 counts per original spectrum. Spectra at the beginning of the series have relatively high amplitude and intermediate FLP, whereas in the course of the measurement, the amplitude subsides with the FLP shifting to the blue; both parameters recover to values close to the initial ones at the end of the series. Notably, the width of a single complex FL spectrum is comparable with that of the bulk spectrum (data not shown). In Fig. 4, two spectra from the same series are compared for better demonstration of the spectral diffusion. In the same figure, we show an example of a fit and the corresponding residuals.

FLP traces

The time course of the FLP of four individual particles is shown in Fig. 5. The spectral integration time is 0.5 s, the excitation intensity at 800 nm is 6 μW, and sample temperature is 20°C. Though acquired with the same excitation intensity and ambient conditions, the traces are qualitatively different. The FLP fluctuates weakly in Fig. 5 A, whereas panels B and C of Fig. 5 demonstrate notable spectral jumps, respectively, to the blue and to the red relative to the initial FLP value. Interestingly, the FLP abruptly jumps between the various levels of almost constant magnitude, and even more remarkably it regains a value close to the initial one before the end of the trace. Unexpectedly, the complex spends a number of seconds in each of the quasi-stable states before it transits to a different state. The trace in Fig. 5 D show spectral diffusion in both directions: the spectrum of this single
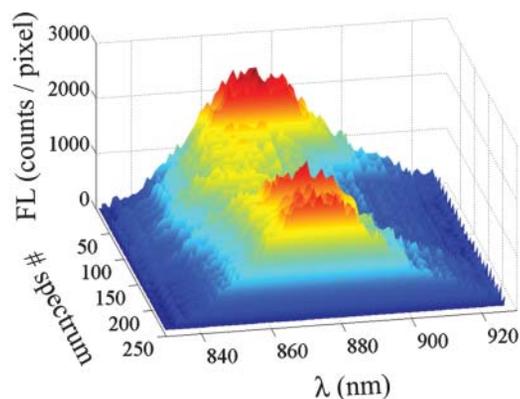

FIGURE 2   FL image of single LH2 complexes immobilized on a poly-L-lysine treated coverslip.

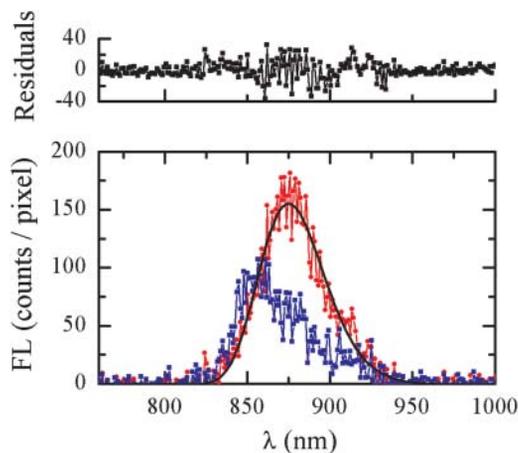FIGURE 3   Series or FL spectra of single LH2.

FIGURE 4 Comparison of two spectra from the original sequence in Fig. 3, with intermediate FLP (*circles*) and blue FLP (*squares*). The solid curve is the skewed Gaussian fit.

complex first drifts to longer wavelengths then abruptly jumps to the blue, finally settling at a FLP, blue-shifted by ∼15 nm relative to the initial FLP, preventing the unambiguous classification of this particle as performing a spectral jump in one direction. We note that these conspicuous spectral jumps are in many cases reversible, and the initial FLP value (or a value close to it) is regained (Fig. 5, *B* and *C*). For other particles, the initial FLP is not recovered before photobleaching occurs (Fig. 5 *D*) (or rather an apparent photobleaching—we have observed the recovery of the emission of some complexes after dark periods longer than 2 min, data not shown). Careful inspection of the trace in Fig. 5 *C* reveals that the LH2 bleaching does not occur as a single event: after entering a dark state for a few seconds, the emission of this complex reappears with a different FLP position. On the other hand, the spectral diffusion can occur without temporary loss of the radiative power as is shown in Fig. 5 *B*.

Spectral fluctuations of different magnitude and frequency were observed depending on the excitation intensity and sample temperature. These fluctuations can naturally occur in the system or they can be induced by elevated temperature or increased excitation intensity. To investigate these possibilities, we have calculated various statistical properties of the obtained spectra.

Single-molecule average and bulk spectra

An average of all spectra measured at 20°C with 6 μW excitation intensity is compared in Fig. 6 with the 500 nW excitation bulk spectrum. The mean of the single-molecule spectra has the same FLP position but is somewhat broader than the bulk spectrum. The broadening of the former is due to the contribution of the particles that underwent spectral shifts either to higher or lower wavelengths. The true bulk spectrum results from a contribution of a much larger number of single
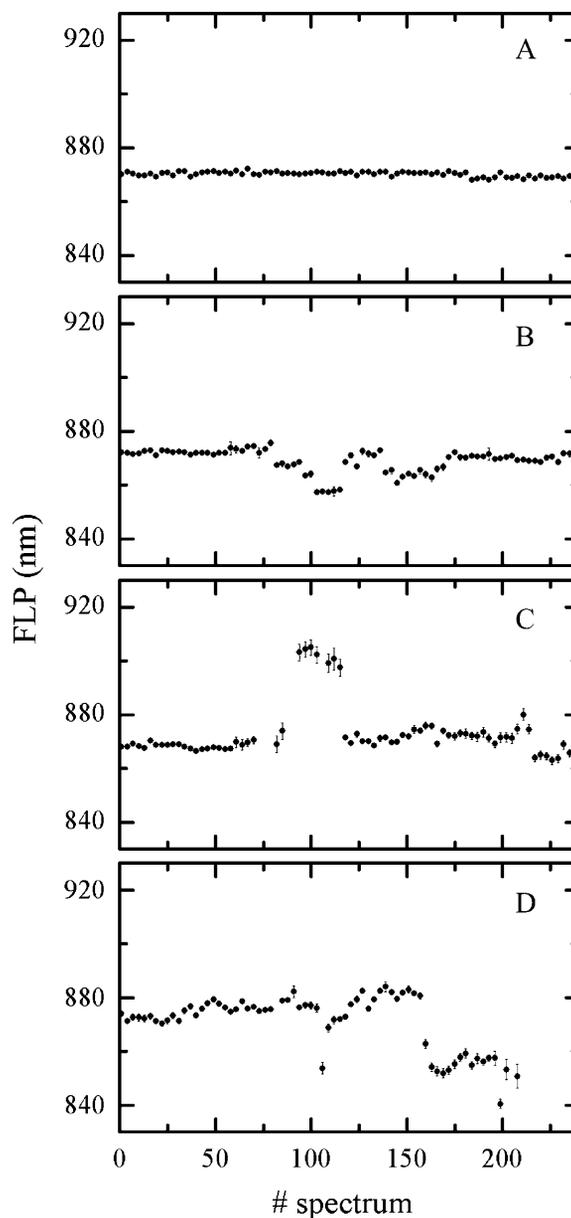
FIGURE 5 FLP time traces of four individual LH2s. Only every third data point is presented to improve clarity. Various spectral diffusion scenarios: (*A*) insignificant diffusion, (*B*) spectral jumps to the blue, (*C*) spectral jump to the red, and (*D*) spectral jumps both to the red and to the blue.

molecules, detected at different stages of evolution in their conformational landscape. Consequently, if the number of the available conformational states were the same for the molecules constituting the bulk and for the particles measured individually, then the bulk and the average spectra would have identical shape (provided sufficient statistics of single-molecule spectra measurements exists). The nonoverlap of the two spectra (even given a limited number of single-molecule measurements) implies that the higher excitation intensity drives the molecules into conformational states less accessible or even unavailable in the dark.
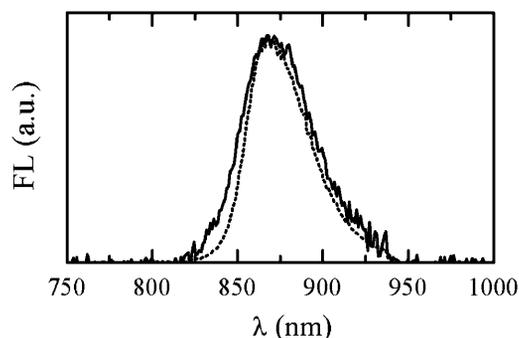
FIGURE 6 Comparison of the 500 nW excitation bulk spectrum (*dotted curve*) with the time and population average (*solid curve*) of single-molecule spectra, acquired with 6 μW excitation.

Distributions of the FLP and the standard deviation of FLP

The excitation intensity and ambient temperature dependence of the observed spectral fluctuations are summarized in histograms of the FLP and the standard deviation of the FLP (SDFP) time traces (Fig. 7). An FLP histogram represents the distribution of the peak wavelengths of all the single-molecule spectra measured under particular experimental conditions. SDFP was calculated for each particle with the original spectral integration time, and is indicative of the FLP fluctuation from the mean value for that particle. The SDFP

distribution reflects the number of strongly fluctuating particles in the particular experimental population. The FLP distribution results partly from the particles having an intrinsically shifted spectrum and partly from the spectral fluctuations. Comparison of FLP histograms obtained at 20°C with 500 nW (Fig. 7 A) and 6 μW (Fig. 7 B) excitation intensity reveals a broadening of the distribution with increasing excitation intensity. This broadening is due to an increased occurrence of significant spectral diffusion. Similarly, comparison of SDFP histograms acquired at 20°C with 500 nW (Fig. 7 D) and 6 μW (Fig. 7 E) indicates notably larger number of particles exhibiting significant and/or frequent spectral jumps at higher excitation intensity. The temperature dependence of spectral fluctuations is also observable though less pronounced. At 35°C and 500 nW excitation (Fig. 7 F), the SDFP distribution is broader than at 20°C and the same excitation intensity (Fig. 7 D), but still much narrower than that, calculated from the measurement at 20°C and 6 μW (Fig. 7 E). Similarly, the FLP distribution resulting from the measurement at 35°C and 500 nW excitation (Fig. 7 C) is broader than the one at 20°C and 500 nW (Fig. 7 A) but notably narrower than at 20°C and 6 μW (Fig. 7 B). Thus, laser light-induced spectral fluctuations are more significant than those associated with experimentally feasible increases in temperature. At temperatures higher than 35°C, the sample preparation deteriorated before the equilibration of the laser focus position could be achieved, thus rendering the collection of data not feasible.
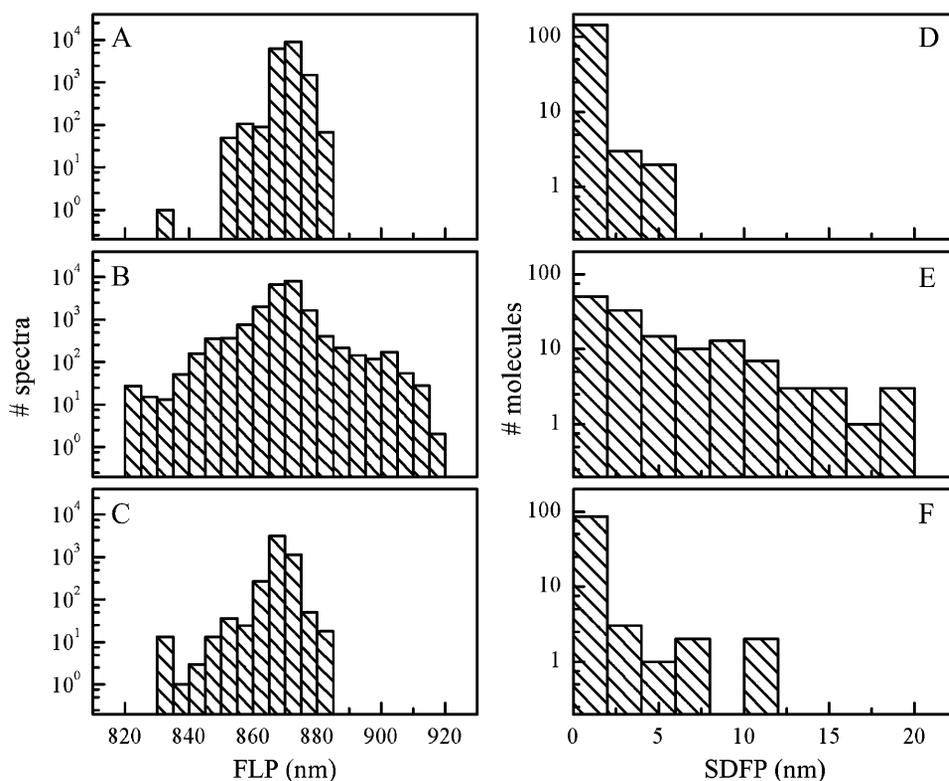

FIGURE 7 Distributions of FLP and SDFP. (*A* and *D*), 20°C and 500 nW excitation; (*B* and *E*), 20°C and 6 μW; and (*C* and *F*), 35°C and 500 nW.

Statistics of strongly fluctuating molecules

Table 1 summarizes overall numbers of measured particles and particles with large SDFP at different experimental conditions. The fraction of strongly fluctuating particles tends to increase with the excitation intensity. To classify spectral jumps, we chose the negative or positive sign of the third moment of the FLP time trace as a criterion of the spectral shift occurring either to the blue or to the red, respectively. The third moment was chosen since it indicates the extent of the distribution of data values around the mean, and its sign reflects the position of the majority of deviating data values with respect to the mean. It appears that the number of the blue-shifting complexes is larger but of the same order of magnitude as that of the red-shifting assemblies. Considering the limited numbers of molecules used in our measurement, we tentatively conclude that there exists roughly the same probability for a particle to undergo big spectral shift in either direction.

Similarly, elevation of temperature leads to the increase of the amount of strongly fluctuating particles. However, the quantitative relationship between the temperature and the overall number of spectrally diffusing particles is not clear. As in the measurements at high excitation intensity, it appears that there are more blue-shifting complexes. However, the temperature dependence of the ratio of the number of molecules jumping either to the red or to the blue cannot be envisaged either. Better measurement statistics at a larger number of temperature points are required for a quantitative assessment of the heating effect. At the moment, it can be concluded that a temperature effect takes place, but it is much less notable than that associated with the increase of the excitation intensity.

Correlation analysis

Some of the light-harvesting assemblies exhibit a strong correlation between the temporal changes of the FLP and the

TABLE 1   Particles undergoing spectral fluctuation*

	Experimental conditions						
Temperature (°C)	20	20	20	20	20	28	35
Excitation (μW)	0.5	1.5	2.5	3.5	6	0.5	0.5
	Numbers of measured particles						
Total	149	124	128	119	138	120	94
SDFP > 2.44							
Total	2	23	32	30	58	8	5
Blue	2	18	17	18	45	4	4
Red	0	5	15	12	13	4	1

The specific value of SDFP of 2.44 is obtained from the 500 nW excitation data set. The major part of corresponding SDFP values is distributed in a narrow range, but a small number of standard deviation values are distinctly separate from the rest (data not shown). The 2.44 value is the maximum of the main part of the distribution and thus thresholds the onset of significant spectral fluctuation.
*Numbers of particles undergoing spectral shift to the blue or to the red are denoted ''blue'' and ''red'', respectively.

amplitude or between the FLP and the fwhm (in the following analysis, correlation is arbitrarily considered strong if its absolute value is in the 0.5–1 range). We observed that these correlations might be either positive or negative. For example, there exist single LH2s that display a negative jump of the FLP with a concomitant increase of the fwhm (negative correlation); others undergo an increase of the FLP that is connected with the increment of the fwhm (positive correlation). Furthermore, some of the molecules are characterized by strong correlations between both pairs of parameters. Fig. 8 presents an example of two individual LH2s with all three parameters progressing in time in a correlated manner. A spectral jump to the blue is accompanied by the increase of the fwhm and the decrement of the amplitude in Fig. 8, D–F. On the other hand, FLP jump to longer wavelengths is again associated with the increment of the fwhm and the reduction of the amplitude in Fig. 8, A–C.

Table 2 summarizes the statistics of particles with large SDFP, featuring strong positive or negative pairwise (either FLP-amplitude or FLP-fwhm) correlations. It also lists the numbers of particles exhibiting a combination of pairwise correlations: either positive FLP-amplitude and negative FLP-fwhm, or negative FLP-amplitude and positive FLP-fwhm. Interestingly, we observed only a few occurrences of molecules indicating a different combination of pairwise correlations. It appears from the table that the proportion of strongly correlating particles relative to the number of strongly fluctuating ones is dependent on the excitation power and generally is significant.

Table 2 also contains information about the particles that show a combination of the pairwise correlations and in addition exhibit a particular sign of the third moment of the FLP time trace. It appears that most of the molecules with the positive FLP-amplitude and negative FLP-fwhm correlations have that sign negative; on the other hand, the negative FLP-amplitude and positive FLP-fwhm combination of the correlations corresponds very well with the third moment being positive. This means that, for example, if the third moment is negative, the FLP drops, spectrum broadens (since the FLP-fwhm correlation is negative, the fwhm has to increase with the reduction of the FLP), and subsides in intensity (since the amplitude-FLP correlation is positive, the decrease of the FLP means the declining amplitude). In fact, the judgment by the third moment in a small number of cases does not coincide with the visual impression of the sign of the spectral jump. Effectively, all the particles exhibiting double pairwise correlation undergo spectral diffusion in the same direction. Overall, we observe that if a particle undergoes significant spectral diffusion, which is accompanied by the correlated evolution of all three spectral fit parameters, then FLP increase or reduction is associated with the spectral broadening and the loss of the radiative power. Furthermore, there exists a very good correspondence between a particle having only strong positive FLP-amplitude or negative FLP-fwhm correlation and its tendency to exhibit
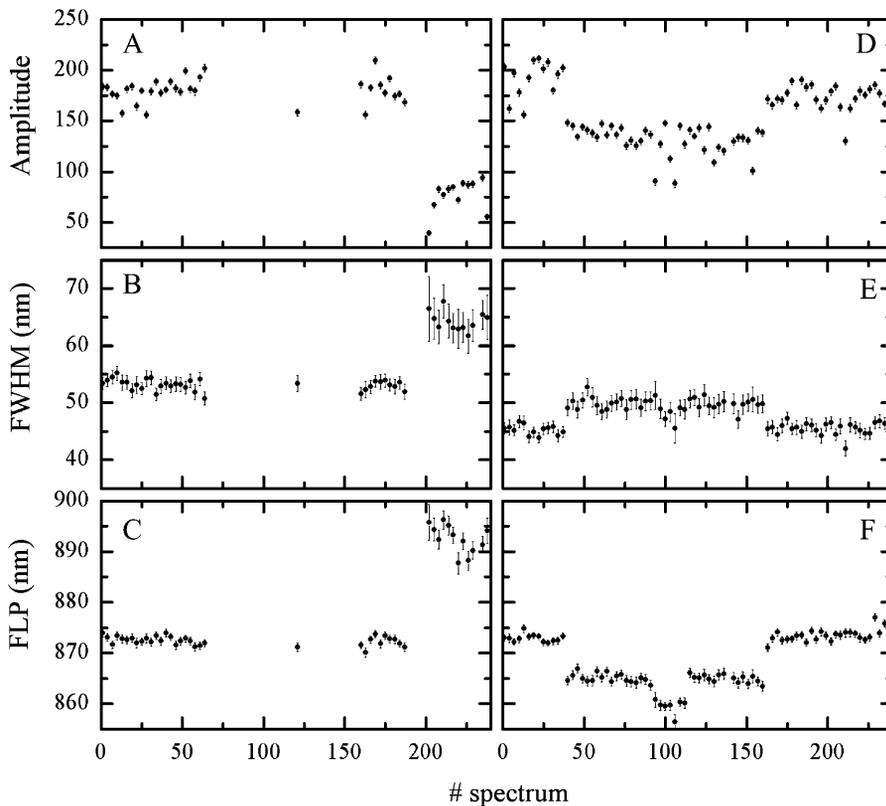
FIGURE 8 Correlated FLP, amplitude, and fwhm traces of two individual LH2s.: (A–C) spectral shift to the red; and (D–F) spectral shift to the blue. Excitation intensity at 800 nm is 6 μW for D–F and 3.5 μW for A–C.

big spectral shifts to the blue; similarly, merely negative FLP-amplitude or positive FLP-fwhm correlation is associated with the red-shifting.

A quantitative relationship between the number of the correlating particles and the excitation intensity is not evident from the data presented here, which is probably due to the limited statistics of our measurement. In fact, even at the highest excitation intensity, only ~10% of the particles exhibit strong correlations. Thus the occurrence of the correlated behavior is generally quite rare. Nevertheless, at the lowest excitation of 500 nW, we observe no particles with two pairwise correlations. Such correlating particles appear with the increase of the excitation intensity though the number of these particles does not increase monotonously with the excitation intensity. Fewer appear as the temperature is increased. Consequently, we are able to conclude that higher levels of excitation, and to a lesser extent increase of an ambient temperature, induce correlated behavior of the particles.

Statistics of spectral jumps

We further characterize the statistics of the spectral jumping by calculating the distributions of jumps of a certain magnitude over the whole population of complexes measured under the same experimental conditions. A threshold of the jump size is arbitrarily set to 2 nm. The magnitude of the jump is calculated between two adjacent points in FLP

time trace. Before the calculation, points of the trace are pooled in bins to yield a time bin of 2 s, common to all the experimental data sets. In Fig. 9, we show histograms of spectral jumps at excitation intensities of 0.5 μW and 6 μW. Distributions of jump size broaden with excitation intensity resulting in exponential decay components of 0.97 ± 0.06

TABLE 2 Molecules exhibiting strong correlations between spectral fit parameters

			Experimental conditions				
Temperature (°C)	20	20	20	20	20	28	35
Excitation (μW)	0.5	1.5	2.5	3.5	6	0.5	0.5
			Numbers of measured particles				
Total	149	124	128	119	138	120	94
SDFP > 2.44	2	23	32	30	58	8	5
			Numbers of correlating particles				
Amplitude-FLP positive	1	11	7	9	19	1	0
FLP-fwhm negative	0	7	5	6	13	1	3
Combination (blue shift)	0 (0)	6 (6)	3 (2)	5 (5)	11 (9)	0 (0)	0 (0)
Amplitude-FLP negative	0	3	3	13	7	2	1
FLP-fwhm positive	0	4	7	13	7	4	1
Combination (red shift)	0 (0)	3 (3)	2 (2)	11 (11)	5 (3)	2 (2)	0 (0)

''Combination (blue shift)'' refers to the number of particles that exhibit both amplitude-FLP and FLP-fwhm correlations with corresponding signs. Numbers in brackets point to the particles that, in addition to both pairwise correlations, have the negative third moment of the FLP time trace. Similarly, ''combination (red shift)'' relates to the corresponding combination of correlations and particles with positive third moment of the FLP time trace.
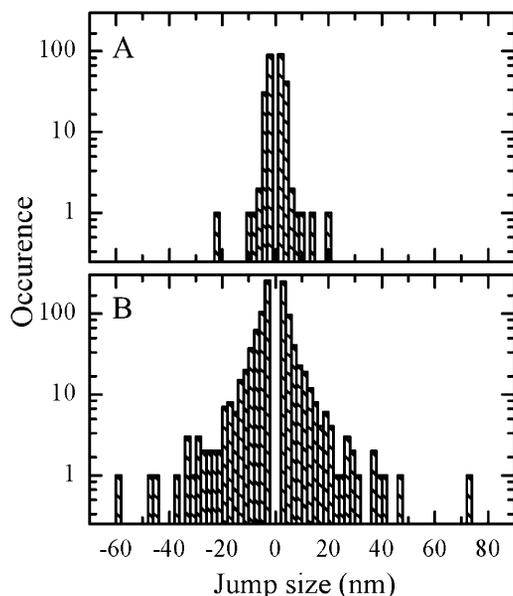
FIGURE 9 Occurrences of spectral jumps of a certain size, calculated over all FLP trajectories measured under the same experimental conditions. Excitation intensity: (A) 0.5 μW and (B) 6 μW.

and −0.69 ± 0.05, and 2.18 ± 0.04 and −2.25 ± 0.08, respectively. Logarithmic representation of a particular jump-size occurrence reveals rare cases of excessively large jumps. The number of such outlier spectral shifts notably increases with excitation intensity.

Finally, the threshold of the jump size was set to 5 nm, and the number of jumps greater than the limiting value was calculated for all the particles for each experimental population. The excitation intensity and temperature dependence of the average number of jumps per molecule is depicted in Fig. 10. For the measurements at 20°C, this number increases approximately linearly with the excitation, which is in agreement with a simple model regarding the transition between two spectrally different conformations of the protein as a local temperature-driven activation process.
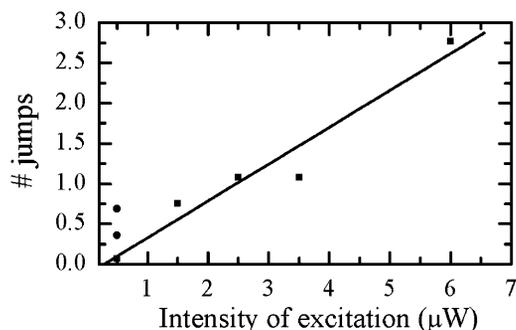

FIGURE 10 Intensity dependence of an average number of spectral jumps exceeding 5 nm calculated over different experimental populations of particles. Square data points with a linear fit correspond to 20°C. Circle data points are acquired with 500 nW excitation at two elevated temperature values: upper point at 28°C, lower point at 35°C.

On the other hand, the increase of the temperature in the experiments with 500 nW excitation power leads to relatively small change of the frequency of spectral shifting. In fact, in our experiment, the number of jumps at 35°C is smaller than that at 28°C, which is probably due to insufficient difference of temperature values. Temperature effect is too weak to obtain a consistent increase in the number of spectral jumps with temperature increase of 7°C. Extrapolation of the experimental data linear-fit, to zero intensity of excitation, indicates a vanishing average number of jumps at that intensity.

DISCUSSION AND MODELING

After the B800 ring in the LH2 complex absorbs an excitation photon, energy is transferred to the B850 BChl molecules in ~1 ps (Ma et al., 1997; Salverda et al., 2000) with a very high efficiency since competing processes of FL and nonradiative decay are three orders of magnitude slower (Monshouwer et al., 1997). Subsequently, exciton relaxation and excitation hopping occur in the B850 ring, with a certain probability leading to FL.

Considering that the molar absorption coefficient of LH2 at 800 nm is 2.3 × 10^6 M^{-1}cm^{-1} (Alden et al., 1997), a single complex will absorb 8.6 × 10^6 photons/s, if positioned in the center of the Gaussian laser beam, delivering 1 μW of CW excitation at 800 nm. The Bchl triplet with a lifetime of 70 μs (Monger et al., 1976) is formed with 2–15% yield (Cogdell et al., 1981; Monger et al., 1976) and is transferred to the carotenoid in ~20 ns (Angerhofer et al., 1995). This transfer step is highly efficient due to a Bchl triplet lifetime much longer than the transfer time. The carotenoid triplet, having a lifetime of ~10 μs (Angerhofer et al., 1995), is a very efficient trap for the singlet Bchl excitations due to singlet-triplet (S-T) annihilation occurring in ~6 ps (Bradforth et al., 1995), since the competing FL and radiationless relaxation processes are much slower. From the simple calculation with the above parameters, it follows that in the presence of the carotenoid triplet in the complex, FL is heavily quenched (~200 times weaker than in the triplet-free condition). Formation of a second triplet in the system is also prevented by the fast S-T annihilation: since the intersystem crossing for the Bchl takes place in 50 ns (calculated from the triplet yield of 0.02 (Monger et al., 1976) and radiative lifetime of 1 ns (Monshouwer et al., 1997)), due to fast S-T annihilation, probability of the second triplet formation is 0.0001. With 1 μW excitation power, it would take 0.1 ms to form the second triplet in the system, which is an order of magnitude longer than the lifetime of the carotenoid triplet.

In summary, the system will spend part of its time in a state with a carotenoid triplet, in which the FL is very weak, and part of the time it will be in the triplet-free state and re-emit with a 10% quantum efficiency (Monshouwer et al., 1997). The resulting quantum efficiency is dependent on the

excitation rate and the yield of triplet formation. Triplet formation frequency is dependent on triplet quantum yield and excitation intensity. Thus, the resulting FL quantum efficiency is dependent on the same set of parameters. At 500 nW excitation intensity, we observe FL count rate of ~8500 counts/s, which with the estimated signal collection efficiency of 8%, corresponds to 9% triplet formation yield (value in the middle of the range cited above). This corresponds to the resulting FL quantum efficiency of 2.5%.

This analysis implies that only a small fraction of the absorbed excitation photons is reemitted as FL. The remaining excitations either decay radiationlessly directly to the ground state, form a triplet, or are quenched by triplets. In these cases, the absorbed excitation energy is eventually dissipated as heat, which leads to local temperature increase of the pigment surroundings. The pigment-protein complex is characterized by an existence of multiple potential energy substates separated by energetic barriers and corresponding to different protein structural conformations. Local temperature increase is a plausible cause of the structural alteration of the protein: in the event of overheating, protein is removed from its local energetic minimum, and upon subsequent cooling due to heat diffusion, it possibly arrives to a state with a different energetic minimum. The change in the protein conformation induces the change in the pigment-protein interaction, which is possibly manifested as spectral change.

From the above analysis of excitation energy dynamics and time traces of the FLP position, it appears that despite the large number of excitations dumped in the system in the form of heat, the complex appears to dwell for a relatively long time in one of the quasi-stable states, characterized by a specific peak position, spectral shape, and intensity of the emission. We thus conclude that the free-energy barriers separating those quasi-stable states with distinctly different spectroscopic properties must be large.

On a phenomenological level, we will associate the possible light-induced structural alterations and their effect on pigment-protein interactions with a change in realization of the static disorder of the electronic transition energies of pigments in the complex, which is in turn connected to particular spectral properties. Below we develop a model that quantitatively describes the observed changes in the spectral profile and position on the basis of this hypothesis.

A quantitative description of single-molecule emission spectra

In our model for the FL spectrum of a single B850 ring, we utilize the modified Redfield approach that incorporates excitonic interactions, static disorder of the electronic transition energies of the pigments, and strong coupling of the electronic transitions to nuclear motions (phonons) of the surrounding (protein) medium. The spectral lineshape of the pigment-protein complex, and its dynamics are determined by coupling of electronic transitions to a manifold of nuclear modes. Fast modes determine the optical lineshape both in conventional (Mukamel, 1995) and single-molecule spectroscopies (Jung et al., 2002). Slow nuclear motions are associated with the evolution of the pigment-protein conformation on a microsecond to second timescale and result in different equilibrium positions of the nuclear coordinates, producing different realizations of the static disorder of the electronic transition energies (Dempster et al., 2001). They are the cause of the inhomogeneous broadening of the bulk spectrum. Particular nuclear coordinates result in specific states for a single complex, characterized by a certain FLP and a lineshape. Thermally activated slow nuclear motions lead to the transitions between these states, observed as abrupt jumps in the FLP traces (Fig. 5). Here we will not consider the dynamics of such transitions, but restrict ourselves to the modeling of the FL lineshapes for different realizations of the disorder.

The energies of the exciton levels are calculated by constructing and diagonalizing the one-exciton Hamiltonian. B850 BChls in the dimeric subunit of LH2 are assumed to have unperturbed transition energies of 12415 and 12215 cm^{-1} (Koolhaas et al., 1997) that were adjusted from a fit of a bulk spectrum. The energies of interactions of pigments associated with proteins 1α-1β, 1α-2α, 1α-2β, 1β-2α, and 1β-2β (the same number denotes the same protein dimer, whereas different numbers denote neighboring dimers), were taken to be 291, −50, 12, 273, and −36 cm^{-1}, respectively (Sauer et al., 1996). The static disorder of the transition energies was taken into account by introducing uncorrelated variations randomly taken from a Gaussian distribution with a fwhm of σ. The numerical diagonalization of the Hamiltonian (for each realization of the disorder) provides the energies of the exciton states, ω_k, and the wave-function amplitudes, c_n^k (participation of the nth pigment site in the kth exciton state).

Relatively high excitation densities we apply in our experiment might produce more than one excitation in a single LH2 complex. We model the B850 ring with one-exciton Hamiltonian, since the emission lifetime is ~1 ns (Monshouwer et al., 1997), whereas much faster exciton annihilation occurs on a picosecond (Ma et al., 1997) timescale, thus making the FL signal contribution from two-exciton states negligible.

The absorption and FL lineshapes of the exciton states are calculated assuming strong exciton-phonon coupling (Zhang et al., 1998). The homogeneous absorption lineshape for the kth exciton state is expressed in terms of the line broadening function, g_k. The steady-state Stokes shift of the emission maximum of the kth state is given by $2\lambda_k$, where λ_k is the reorganization energy. Both g_k and λ_k are related to the spectral density, $C_k(\omega)$, in the exciton basis, which is connected with the spectral density in the site representation, $C_n(\omega)$, through the fourth power of the wave-function amplitudes, i.e., $C_k(\omega) = \sum_n (c_n^k)^4 C_n(\omega)$. Here we have assumed that the phonon-induced fast modulation of the

electronic transitions is described by an uncorrelated diagonal disorder (not to be confused with the static disorder). The $\sum_n (c_n^k)^4$ factor is also known as the participation ratio (PR), or inverse delocalization length of the kth exciton state. Indeed, the PR of the exciton state is relatively small only if all of the wave-function amplitudes are small, which, due to the normalization condition, guarantees approximately equal contributions from different sites and is indicative of excitation delocalization over different sites. On the other hand, again due to the normalization requirement, a large PR could result only from a few relatively large and remaining small wave-function amplitudes, implying that the excitation is localized on a few sites predominantly contributing to the value of PR.

In summary, the phonon-induced broadening and the Stokes shift of each of the exciton levels is dependent on the PR of that level, which in turn is dependent on the realization of the static disorder through the wave-function amplitudes. Hence, the optical lineshape and the peak position are determined by the realization of the static disorder.

The spectral density $C_n(\omega)$ is assumed to have the form of an overdamped Brownian oscillator (Mukamel, 1995; Zhang et al., 1998) with the coupling parameter λ and relaxation time τ. In our model, λ and τ (as well as σ) are site-independent free parameters adjusted from the fit of the absorption and FL spectra. The RT single-molecule FL spectrum, acquired with 6 μW excitation intensity and averaged in time and over particles together with the distribution of the FL peak positions (Fig. 11), can be reproduced with $\sigma = 370$ cm^{-1}, $\lambda = 390$ cm^{-1}, and $\tau = 50$ fs. Notably, the RT absorption spectrum of the LH2 B850 band in vivo can be reproduced with the same σ and τ, and $\lambda = 220$ cm^{-1} (data not shown).

The model also takes into account the relaxation-induced broadening, i.e., we suppose an additional homogeneous broadening of the exciton states given by their inverse lifetimes $R_k = -\sum_{k'} R_{k'k'kk}$, where $R_{k'k'kk}$ is the rate of the $k \rightarrow k'$ transition calculated (Zhang et al., 1998) in terms of g_k functions.

Single LH2 FL profiles calculated for 200 realizations of the static disorder at RT are presented in Fig. 12. The FLP positions are distributed over a range of values similar to the experimental data. However, since we do not have an explicit model to describe the dynamics of spectral jumping, the collection of calculated FLP values does not represent temporal evolution of the spectrum. The average of the calculated FL profiles has a maximum near 870 nm, which is the peak position of the experimental bulk spectrum. Realizations with the FLP near this wavelength occur with the highest probability.

Fig. 13 shows three experimental and corresponding simulated FL profiles with different peak positions. Experimental curves are averages of all single-molecule FL spectra measured with 3.5 μW excitation intensity and featuring FLP in intervals of 859–861, 869–871, and 889–891 nm. These average spectra have respective fwhms of 53, 48, and 67 nm. Simulated profiles are averages of spectra calculated
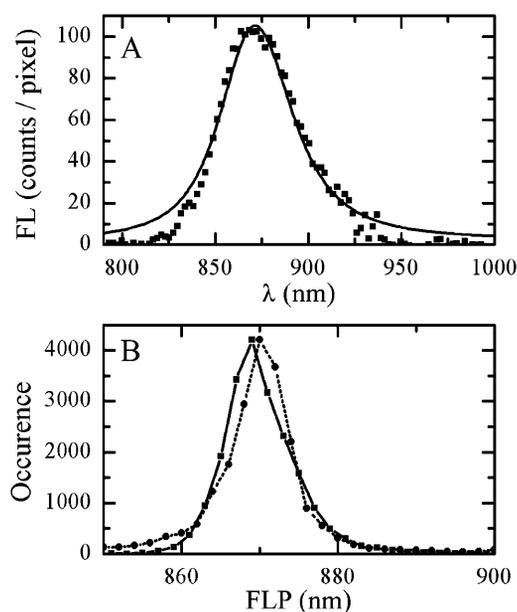
FIGURE 11   (A) An average in time and over experimental population of single-molecule spectra measured with 6 μW excitation intensity at 800 nm (*squares*) and calculated FL spectrum averaged over realizations of static disorder (*solid line*). (B) Distributions of FLP of single-molecule spectra measured with 6 μW excitation intensity at 800 nm (*circles*, *dotted line* to guide the eye) and simulated spectra, calculated with different realizations of disorder (*squares*, *solid line*).

with different realizations of disorder and peaking in the same corresponding intervals. The red-shifted profile has a pronounced short-wavelength wing. Averages with blue-shifted and intermediate FLP positions feature a regular FL profile asymmetry, i.e., a broader long-wavelength tail. Notably, the blue- and red-shifted experimental spectra are broader than that with the intermediate FLP position. Overlaying of experimental and simulated spectra shows that the model satisfactorily reproduces many of the features observed in the experimental data. Typical blue- and red-shifted simulated FL profiles also have lower intensity than the ones with the intermediate FLP (Rutkauskas et al., 2004). Thus simulated spectra qualitatively reproduce the
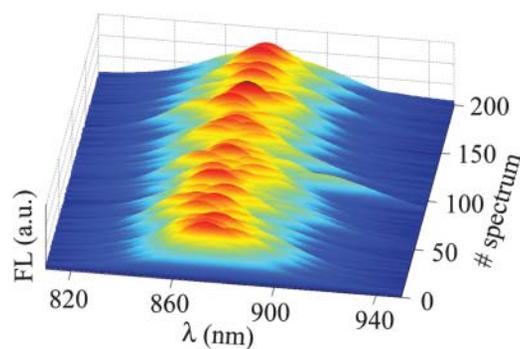

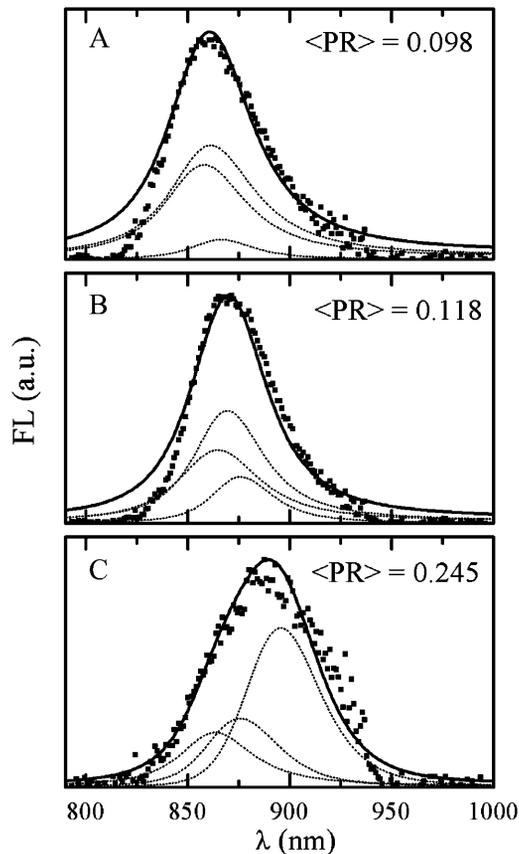FIGURE 12   FL profiles of single LH2 calculated for 200 realizations of disorder at RT.

FIGURE 13 Three spectrally different average experimental (*squares*) and calculated (*solid line*) FL profiles: (*A*) blue-shifted, (*B*) intermediate, and (*C*) red-shifted. Calculated spectra are presented together with contributions from the three lowest exciton components (*dotted lines*).

experimentally observed correlation between spectral peak position shifts and spectral broadening and diminishing intensity.

In the following, we will comment on the mechanism by which static disorder determines the spectral profile shape and peak position. We found that simulated lineshapes with different FLP positions correspond to a specific exciton structure (energy level scheme of exciton states), which in turn is associated with a particular pattern of static disorder. Contributions of the three lowest exciton states to the FL profiles with intermediate, blue-, and red-shifted FLP are depicted by dotted lines in Fig. 13. In this picture, a separate exciton level profile (as well as the whole FL profile) is an average over different realizations of static disorder that result in a FLP within a particular interval. Transition dipole strengths of exciton states are weighed with the steady-state populations of the corresponding exciton states. The three types of exciton structure presented in Fig. 13 correspond to different degrees of excitation delocalization in all three exciton levels. The extent of delocalization can be characterized by a PR of an individual exciton state in the presence of a particular realization of disorder. For a circular aggregate of N molecules, PR = $1/N$ for the lowest and $3/2N$ for higher

states in the absence of the static disorder. In the case of the LH2 ring, $N = 18$ and PR is calculated to be 0.056 and 0.083, respectively. Including the disorder results in a dramatic increase of PR of all states, especially of the lowest one. Even small disorder results in PR = 0.09–0.1 (depending on the realization of the disorder) of all three states. A strongly disordered aggregate is conveniently characterized by a wavelength-dependent participation ratio, PR(λ), defined as the PR average over the exciton states that result from different realizations of the static disorder and feature energies within a narrow interval around λ (Alden et al., 1997; Novoderezhkin et al., 1999a). For example, for LH2, taking interaction energy 250–400 cm^{-1} with a realistic value of disorder of 300–450 cm^{-1} for a fwhm of the Gaussian distribution (Alden et al., 1997; Novoderezhkin et al., 1999b), PR(λ) is almost constant (0.1–0.12) throughout the absorption band (i.e., in the region determined mostly by higher excitonic states), increases to 0.12–0.2 in the red edge, where the lowest state starts to contribute, and increases up to 0.3–0.4 in the very red edge due to the contribution of strongly red-shifted and localized lowest states (Alden et al., 1997; Novoderezhkin et al., 1999a,b, 2003). Delocalization of the exciton states contributing to the steady-state FL is reflected in the thermally averaged participation ratio, $\langle PR \rangle$, defined as an average of individual exciton state PR values weighed with steady-state populations of those states. $\langle PR \rangle$ values corresponding to blue-, intermediate, and red-shifted FLP positions are 0.098, 0.118, and 0.245, respectively, reflecting the increasingly localized character of the exciton states contributing to FL spectrum, when it shifts to the red.

Fig. 13 *A* reveals that the blue-shifted FL profile corresponds to a relatively delocalized exciton ($\langle PR \rangle < 0.1$) with its structure marginally affected by the presence of the static disorder. The lowest $k = 0$ state is only weakly allowed, so the RT emission originates mostly from the degenerate $k = \pm 1$ pair giving rise to a blue-shifted FL.

Notice that k-notation originates from the exciton wavenumbers of a circular aggregate without disorder. For a disordered antenna, mixing of the zero-order wavefunctions produces more complicated exciton states, which cannot be characterized by k wavenumbers. On the other hand, exciton structure of antenna with intermediate values of disorder resembles that of the homogeneous aggregate: larger part of dipole strength is still concentrated in the two higher levels. Thus, for the ease of discussion, we persist in labeling exciton levels with k wavenumbers though they do not have the same meaning for homogeneous and for disordered aggregates.

Realizations of a larger static disorder (Fig. 13 *B*) result in a larger splitting between the $k = \pm 1$ levels, so that the lower $k = -1$ state becomes more populated and more emitting as compared to the $k = 1$. However, both $k = -1$ and $k = 1$ levels still remain delocalized (PR(λ) = 0.09–0.11 in the corresponding spectral region). The lowest $k = 0$ state becomes more emitting, borrowing part of the dipole

strength from higher levels through disorder-induced mixing of states. Due to this mixing, the $k = 0$ state also becomes more localized. The contribution of the lowest state increases $PR(\lambda)$ in the long-wavelength region ($PR(\lambda) = 0.11$–0.17). The corresponding $\langle PR \rangle$ value is ~0.12. Such an exciton structure is characteristic of realizations with the FLP near the maximum of the average emission.

Fig. 13 *C* demonstrates an example of a red-shifted FL profile. Its exciton structure is strongly affected by the disorder, which induces large splitting between the three lowest states. The $PR(\lambda)$ value is large for all the states, especially for the lowest one. Due to the large splitting between the exciton states, the FL originates from the most populated lowest state, which is now strongly allowed and localized ($PR(\lambda) > 0.3$). Its localized character leads to a significant broadening and red shift of the FLP.

Red-shifted FL profiles correspond to a disorder-induced localization of exciton state on 3–4 pigments. Energetic shift of just one pigment in a ring will not lead to such strong localization, since the remaining energetically equivalent and excitonically interacting pigments will give rise to delocalized excitonic state. On the other hand, random energetic shift of a larger number of pigments in the ring will be associated with significantly more pronounced destruction of delocalization of excitonic wavefunction and hence red shift of FL spectrum. Red shift of a few pigments would also shift the overall spectral profile to the red without destruction of exciton delocalization. However, such shift would not be accompanied by the change of spectral shape, since broadening of spectral profile is associated with increased localization.

Downhill exciton relaxation with a rate increasing for the higher levels is an additional line-broadening factor contributing to the width of the blue-shifted FL spectrum. In fact, ''downhill'' relaxation is a result of multiple pathways including both uphill and downhill excitation transfers. However, at finite temperature, the downhill channel is always faster, so the higher states have shorter lifetimes. In our model, $R_k = 16, 29, 44,$ and $57 \, \text{ps}^{-1}$ for $k = 0, -1, 1,$ and -2 levels, respectively. It should be noted that the relaxation tensor in our modeling is different for different realizations of disorder. The inverse lifetimes R_k listed here are averages over disorder.

The more pronounced relaxation broadening of the $k = \pm 1$ levels results in a larger width of the blue-shifted FL spectra (determined mostly by the $k = \pm 1$ emission). Notice that disregarding the relaxational broadening, a blue shift would be always accompanied by the narrowing of the FL line, because the $k = \pm 1$ levels are narrower than the lowest one due to smaller PR values and, as a result, smaller phonon coupling. Omitting the relaxation, it would be impossible to interpret the observed broadening of the blue-shifted FL profile.

CONCLUSIONS

We have experimentally observed notable light-induced jumps of single LH2 FL spectrum peak position between the levels of distinctly different magnitude. Though spectral fluctuations were evidently light-induced, they did not signal the deterioration of the assembly, since in most cases jumps were reversible. We conclude that the intense excitation drives the complex into conformational states, which are less accessible in dark conditions but still intrinsic to the system. The probability for a complex to undergo a large spectral jump either to longer or shorter wavelengths was found to be roughly the same. The number of spectral jumps was found to be linearly dependent on the excitation intensity, which is in agreement with a simple model regarding the transition between two spectrally different conformations of the protein as a local temperature-driven activation process.

The observed spectral jumps were accompanied by a broadening of the FL profile and the decrease of amplitude. We have qualitatively accounted for these effects by modeling the FL with different realizations of the static disorder of pigment transition energies. However, our model does not encompass the dynamics of the spectral jumps. The observation that large spectral jumps occur with a very low probability with respect to the number of excitations received by the system leads us to conclude that large free-energy barriers separate the states with distinctly different spectral properties.

REFERENCES

Alden, R. G., E. Johnson, V. Nagarajan, W. W. Parson, C. J. Law, and R. J. Cogdell. 1997. Calculations of spectroscopic properties of the LH2 bacteriochlorophyll-protein antenna complex from Rhodopseudomonas acidophila. *J. Phys. Chem. B*. 101:4667–4680.

Angerhofer, A., F. Bornhauser, A. Gall, and R. J. Cogdell. 1995. Optical and optically detected magnetic-resonance investigation on purple photosynthetic bacterial antenna complexes. *Chem. Phys.* 194:259–274.

Bopp, M. A., Y. W. Jia, L. Q. Li, R. J. Cogdell, and R. M. Hochstrasser. 1997. Fluorescence and photobleaching dynamics of single light-harvesting complexes. *Proc. Natl. Acad. Sci. USA*. 94:10630–10635.

Bopp, M. A., A. Sytnik, T. D. Howard, R. J. Cogdell, and R. M. Hochstrasser. 1999. The dynamics of structural deformations of immobilized single light-harvesting complexes. *Proc. Natl. Acad. Sci. USA*. 96:11271–11276.

Bradforth, S. E., R. Jimenez, F. van Mourik, R. van Grondelle, and G. R. Fleming. 1995. Excitation transfer in the core light-harvesting complex (Lh-1) of rhodobacter-sphaeroides: an ultrafast fluorescence depolarization and annihilation study. *J. Phys. Chem.* 99:16179–16191.

Cogdell, R. J., P. K. Fyfe, S. J. Barrett, S. M. Prince, A. A. Freer, N. W. Isaacs, P. McGlynn, and C. N. Hunter. 1996. The purple bacterial photosynthetic unit. *Photosynth. Res.* 48:55–63.

Cogdell, R. J., and A. M. Hawthornthwaite. 1993. Preparation, purification and crystallization of purple bacterial antenna complexes. *In* The Photosynthetic Reaction Center. J. R. Norris and J. Deisenhofer, editors. Academic Press, New York: 23–42.

Cogdell, R. J., M. F. Hipkins, W. MacDonald, and T. G. Truscott. 1981. Energy transfer between the carotenoid and the bacteriochlorophyll within the B-800–850 light-harvesting pigment-protein complex of *Rhodopseudomonas shaeroides*. *Biochim. Biophys. Acta*. 634:191–202.

Dempster, S. E., S. J. Jang, and R. J. Silbey. 2001. Single molecule spectroscopy of disordered circular aggregates: a perturbation analysis. *J. Chem. Phys.* 114:10015–10023.

Fowler, G. J. S., R. W. Visschers, G. G. Grief, R. van Grondelle, and C. N. Hunter. 1992. Genetically modified photosynthetic antenna complexes with blueshifted absorbency bands. *Nature*. 355:848–850.

Frauenfelder, H. 2003. Complexity of Proteins. Physics of Biological Systems: From Molecules to Species. Springer-Verlag, Heidelberg, Germany.

Gerken, U., F. Jelezko, B. Gotze, M. Branschadel, C. Tietz, R. Ghosh, and J. Wrachtrup. 2003. Membrane environment reduces the accessible conformational space available to an integral membrane protein. *J. Phys. Chem. B*. 107:338–343.

Halloren, E., G. McDermott, J. G. Lindsay, C. Miller, A. A. Freer, N. W. Isaacs, and R. J. Cogdell. 1995. Studies on the light-harvesting complexes from the thermotolerant purple bacterium *Rhodopseudomonas-cryptolactis*. *Photosynth. Res.* 44:149–155.

Hofmann, C., T. J. Aartsma, H. Michel, and J. Kohler. 2003. Direct observation of tiers in the energy landscape of a chromoprotein: a single-molecule study. *Proc. Natl. Acad. Sci. USA*. 100:15534–15538.

Hu, X. C., T. Ritz, A. Damjanovic, F. Autenrieth, and K. Schulten. 2002. Photosynthetic apparatus of purple bacteria. *Q. Rev. Biophys.* 35:1–62.

Hu, X. C., T. Ritz, A. Damjanovic, and K. Schulten. 1997. Pigment organization and transfer of electronic excitation in the photosynthetic unit of purple bacteria. *J. Phys. Chem. B*. 101:3854–3871.

Jung, Y., E. Barkai, and R. J. Silbey. 2002. Current status of single-molecule spectroscopy: Theoretical aspects. *J. Chem. Phys.* 117:10980–10995.

Ketelaars, M., A. M. van Oijen, M. Matsushita, J. Köhler, J. Schmidt, and T. J. Aartsma. 2001. Spectroscopy on the B850 band of individual light-harvesting 2 complexes of *Rhodopseudomonas acidophila*. I. Experiments and Monte Carlo simulations. *Biophys. J.* 80:1591–1603.

Koolhaas, M. H. C., G. van der Zwan, R. N. Frese, and R. van Grondelle. 1997. Red shift of the zero crossing in the CD spectra of the LH2 antenna complex of *Rhodopseudomonas acidophila*: a structure-based study. *J. Phys. Chem. B*. 101:7262–7270.

Ma, Y. Z., R. J. Cogdell, and T. Gillbro. 1997. Energy transfer and exciton annihilation in the B800–850 antenna complex of the photosynthetic purple bacterium *Rhodopseudomonas acidophila* (Strain 10050). A femtosecond transient absorption study. *J. Phys. Chem. B*. 101:1087–1095.

Matsushita, M., M. Ketelaars, A. M. van Oijen, J. Köhler, T. J. Aartsma, and J. Schmidt. 2001. Spectroscopy on the B850 band of individual light-harvesting 2 complexes of *Rhodopseudomonas acidophila*. II. Exciton states of an elliptically deformed ring aggregate. *Biophys. J.* 80:1604–1614.

McDermott, G., S. M. Prince, A. A. Freer, A. M. Hawthornthwaite-Lawless, M. Z. Papiz, R. J. Cogdell, and N. W. Isaacs. 1995. Crystal-structure of an integral membrane light-harvesting complex from photosynthetic bacteria. *Nature*. 374:517–521.

Monger, T. G., R. J. Cogdell, and W. W. Parson. 1976. Triplet states of bacteriochlorophyll and carotenoids in chromatophores of photosynthetic bacteria. *Biochim. Biophys. Acta*. 449:136–153.

Monshouwer, R., M. Abrahamsson, F. van Mourik, and R. van Grondelle. 1997. Superradiance and exciton delocalization in bacterial photosynthetic light-harvesting systems. *J. Phys. Chem. B*. 101:7241–7248.

Mukamel, S. 1995. Principles of Nonlinear Optical Spectroscopy. Oxford University Press, New York.

Novoderezhkin, V., R. Monshouwer, and R. van Grondelle. 1999a. Disordered exciton model for the core light-harvesting antenna of *Rhodopseudomonas viridis*. *Biophys. J.* 77:666–681.

Novoderezhkin, V., R. Monshouwer, and R. van Grondelle. 1999b. Exciton (de)localization in the LH2 antenna of *Rhodobacter sphaeroides* as revealed by relative difference absorption measurements of the LH2 antenna and the B820 subunit. *J. Phys. Chem. B*. 103:10540–10548.

Novoderezhkin, V., M. Wendling, and R. van Grondelle. 2003. Intra- and interband transfers in the B800–B850 antenna of *Rhodospirillum molischianum*: Redfield theory modeling of polarized pump-probe kinetics. *J. Phys. Chem. B*. 107:11534–11548.

Olsen, J. D., G. D. Sockalingum, B. Robert, and C. N. Hunter. 1994. Modification of a hydrogen-bond to a bacteriochlorophyll-a molecule in the light-harvesting 1-antenna of *Rhodobacter-sphaeroides*. *Proc. Natl. Acad. Sci. USA*. 91:7124–7128.

Papiz, M. Z., S. M. Prince, T. Howard, R. J. Cogdell, and N. W. Isaacs. 2003. The structure and thermal motion of the B800–850 LH2 complex from *Rps. acidophila* at 2.0 Å over-circle resolution and 100 K: new structural features and functionally relevant motions. *J. Mol. Biol.* 326:1523–1538.

Robert, B., R. J. Cogdell, and R. van Grondelle. 2003. Light-harvesting antennas in photosynthesis. B. R. Green and W. W. Parson, editors. *In* Light-Harvesting Antennas in Photosynthesis. Kluwer Academic Publishers, Dordrecht, The Netherlands. 169–194.

Rutkauskas, D., V. Novoderezkhin, R. J. Cogdell, and R. van Grondelle. 2004. Fluorescence spectral fluctuations of single LH2 complexes from *Rhodopseudomonas acidophila* strain 10050. *Biochemistry*. 43:4431–4438.

Salverda, J. M., F. van Mourik, G. van der Zwan, and R. van Grondelle. 2000. Energy transfer in the B800 rings of the peripheral bacterial light-harvesting complexes of *Rhodopseudomonas acidophila* and *Rhodospirillum molischianum* studied with photon echo techniques. *J. Phys. Chem. B*. 104:11395–11408.

Sauer, K., R. J. Cogdell, S. M. Prince, A. Freer, N. W. Isaacs, and H. Scheer. 1996. Structure-based calculations of the optical spectra of the LH2 bacteriochlorophyll-protein complex from *Rhodopseudomonas acidophila*. *Photochem. Photobiol.* 64:564–576.

Scheuring, S., F. Reiss-Husson, A. Engel, J. L. Rigaud, and J. L. Ranck. 2001. High-resolution AFM topographs of *Rubrivivax gelatinosus* light-harvesting complex LH2. *EMBO J.* 20:3029–3035.

Scholes, G. D., and G. R. Fleming. 2000. On the mechanism of light harvesting in photosynthetic purple bacteria: B800 to B850 energy transfer. *J. Phys. Chem. B*. 104:1854–1868.

Sundström, V., T. Pullerits, and R. van Grondelle. 1999. Photosynthetic light-harvesting: reconciling dynamics and structure of purple bacterial LH2 reveals function of photosynthetic unit. *J. Phys. Chem. B*. 103:2327–2346.

van Grondelle, R. 1985. Excitation energy transfer, trapping and annihilation in photosynthetic systems. *Biochim. Biophys. Acta*. 811:147–195.

van Grondelle, R., J. P. Dekker, T. Gillbro, and V. Sundström. 1994. Energy-transfer and trapping in photosynthesis. *Biochim. Biophys. Acta*. 1187:1–65.

van Grondelle, R., and V. Novoderezhkin. 2001. Dynamics of excitation energy transfer in the LH1 and LH2 light-harvesting complexes of photosynthetic bacteria. *Biochemistry*. 40:15057–15068.

van Oijen, A. M., M. Ketelaars, J. Köhler, T. J. Aartsma, and J. Schmidt. 1999. Unraveling the electronic structure of individual photosynthetic pigment-protein complexes. *Science*. 285:400–402.

van Oijen, A. M., M. Ketelaars, J. Köhler, T. J. Aartsma, and J. Schmidt. 2000. Spectroscopy of individual light-harvesting 2 complexes of *Rhodopseudomonas acidophila*: diagonal disorder, intercomplex heterogeneity, spectral diffusion, and energy transfer in the B800 band. *Biophys. J.* 78:1570–1577.

Wu, H. M., M. Rätsep, I. J. Lee, R. J. Cogdell, and G. J. Small. 1997. Exciton level structure and energy disorder of the B850 ring and the LH2 antennal complex. *J. Phys. Chem. B*. 101:7654–7663.

Zhang, W. M., T. Meier, V. Chernyak, and S. Mukamel. 1998. Exciton-migration and three-pulse femtosecond optical spectroscopies of photosynthetic antenna complexes. *J. Chem. Phys.* 108:7763–7774.